HHS Public Access

Author manuscript

Leukemia. Author manuscript; available in PMC 2022 April 01.

Published in final edited form as:

Leukemia. 2021 August ; 35(8): 2285–2298. doi:10.1038/s41375-021-01166-9.

Cytoplasmic DROSHA and Non-canonical Mechanisms of MiR-155 Biogenesis in FLT3-ITD Acute Myeloid Leukemia

Le Xuan Truong Nguyen[1,‡,*], **Bin Zhang**[1,‡], **Dinh Hoa Hoang**[1], **Dandan Zhao**[1], **Huafeng Wang**[1], **Herman Wu**[1], **Yu-Lin Su**[2], **Haojie Dong**[1], **Sonia Rodriguez-Rodriguez**[1], **Brian Armstrong**[3], **Lucy Y. Ghoda**[1], **Danilo Perrotti**[4], **Flavia Pichiorri**[1], **Jianjun Chen**[5], **Ling Li**[1], **Marcin Kortylewski**[2], **Russell C. Rockne**[1], **Ya-Huei Kuo**[1], **Samer Khaled**[1], **Nadia Carlesso**[1], **Guido Marcucci**[1,*]

[1]Gehr Family Center for Leukemia Research, Hematology Malignancies and Stem Cell Transplantation Institute, City of Hope Medical Center, Duarte, California, USA.

[2]Department of Immuno-Oncology, City of Hope Medical Center, Duarte, California, USA.

[3]Light Microscopy Core, Beckman Research Institute, City of Hope Medical Center, Duarte, California, USA.

[4]Department of Medicine, Biochemistry and Molecular Biology and the Marlene and Greenebaum Comprehensive Cancer Center, University of Maryland, Baltimore, Maryland, USA

[5]Department of System Biology, City of Hope Medical Center, Duarte, California, USA

Abstract

We report here on a novel pro-leukemogenic role of FMS-like tyrosine kinase 3-internal tandem duplication (FLT3-ITD) that interferes with microRNAs (miRNAs) biogenesis in acute myeloid leukemia (AML) blasts. We showed that FLT3-ITD interferes with the canonical biogenesis of intron-hosted miRNAs like miR-126, by phosphorylating SPRED1 protein and inhibiting the "gatekeeper" Exportin 5 (XPO5)/RAN-GTP complex that regulates the nucleus-to-cytoplasm transport of pre-miRNAs for completion of maturation into mature miRNAs. Of note, despite the blockage of "canonical" miRNA biogenesis, miR-155 remains upregulated in FLT3-ITD+ AML blasts, suggesting activation of alternative mechanisms of miRNA biogenesis that circumvent the XPO5/RAN-GTP blockage. MiR-155, a BIC-155 long noncoding (lnc) RNA-hosted oncogenic

[*]Correspondence: Guido Marcucci, MD, Chair and Professor, Department of Hematologic Malignancies Translational Science, City of Hope Medical Center and Beckman Research Institute, 1500 E Duarte Rd, Duarte CA 91010, gmarcucci@coh.org, Phone: (626) 218-2705, Fax: (626) 301-8973Le Xuan Truong Nguyen, PhD, Department of Hematologic Malignancies Translational Science, City of Hope Medical Center and Beckman Research Institute, 1500 E Duarte Rd, Duarte CA 91010, lenguyen@coh.org, Phone: (626) 218-2705, Fax: (626) 301-8973.

[‡]These authors contributed equally to this work

Authors' Contributions

Conception and design: L.X.T.N., B.Z., Y.K., N.C., and G.M.

Development of methodology: L.X.T.N., B.Z., D.H.H., H.W., D.Z., H.W., Y.S., S.R., and H.D.

Acquisition of data: L.X.T.N., B.Z., and G.M.

Providing intellectual inputs: B.A., L.G., D.P., F.P., J.C., L.L., M.K., R.R., and S.K.K.

Writing, review and/or revision of the manuscript: L.X.T.N. and G.M.

Disclosure of Potential Conflicts of Interest

The authors declare that there is no conflict of interest regarding the publication of this article.

miRNA, has previously been implicated in FLT3-ITD+ AML blast hyperproliferation. We showed that FLT3-ITD upregulates miR-155 by inhibiting DDX3X, a protein implicated in the splicing of lnc-RNAs, via p-AKT. Inhibition of DDX3X increases unspliced BIC-155 which is then shuttled by NXF1 from the nucleus to the cytoplasm, where it is processed into mature miR-155 by cytoplasmic DROSHA, thereby bypassing the XPO5/RAN-GTP blockage via “non-canonical” mechanisms of miRNA biogenesis.

Keywords

Acute Myeloid Leukemia (AML); FLT3-ITD; miR-126; miR-155; DROSHA; DDX3X; SPRED1

Introduction

MicroRNAs (miRNAs) are small noncoding RNAs that control gene expression by binding to cognate sites in the 3′ untranslated region (3′ UTR) of target messenger RNAs (mRNAs) [1]. MiRNA coding sequences are hosted in intragenic or intergenic regions of the genome and are transcribed as primary (pri) miRNAs and processed into precursor (pre) miRNAs by nuclear DROSHA before being exported into the cytoplasm via the Exportin 5 (XPO5)/RAN-GTP complex. In the cytoplasm, pre-miRNAs are processed by Dicer into mature miRNAs and incorporated into the RNA-induced silencing complex (RISC), where they pair with target mRNAs to promote their degradation and/or inhibit their translation into the corresponding encoded proteins [1].

We and others previously reported on the biological, prognostic and therapeutic roles of individual miRNAs in acute myeloid leukemia (AML), a genetically heterogeneous myeloid malignancy characterized by differentiation arrest and proliferation of transformed hematopoietic stem and progenitor cells (HSPCs) [2,3,4]. Of note, certain molecular subsets of AML have been associated with deregulated expression of specific miRNAs [5]. To this end, the FMS-like tyrosine kinase 3 *(FLT3)* gene encodes a protein member of the receptor tyrosine kinase (RTK) family that promotes proliferation and survival of normal hematopoietic cells in response to FLT3 ligand binding. In approximately 25% of AML patients, however, the *FLT3* gene acquires an internal tandem duplication (ITD) and encodes a mutant receptor with aberrant, ligand-independent tyrosine kinase (TK) activity that confers growth and survival advantages to leukemic blasts [6]. In the clinic, FLT3-ITD positive (+) AML patients are treated with TK inhibitors (TKIs) in combination with chemotherapy [7]. In FLT3-ITD+ AML, miR-155 has emerged as one of the most significantly upregulated miRNAs and has been shown to play a dosage-dependent role in the hyperproliferation of leukemic blasts that characterizes this molecular subset of the disease [8,9,10,11].

More recently, we and others reported that aberrant TK activity inhibits canonical miRNA biogenesis in leukemia. Using models of chronic myelogenous leukemia (CML), we showed that BCR/ABL downregulates miR-126, by inhibiting the XPO5/RAN-GTP complex and halting miRNA maturation [12,13,14,15,16]. Since higher levels of miR-126 associated with cell quiescence, miR-126 downregulation ultimately promoted leukemia growth [16].

Herein, we hypothesize that by virtue of its aberrant TK activity and similarly to BCR/ABL, FLT3-ITD may also alter miRNA biogenesis by inhibiting the XPO5/RAN-GTP complex. Corollary to this hypothesis is that FLT3-ITD must also activate other mechanisms of miRNA biogenesis to circumvent the "self-imposed" XPO5/RAN-GTP inhibition and allow for miR-155 upregulation as commonly observed in FLT3-ITD+ AML blasts.

Using an AML *Mll*$^{PTD/wt}$/*Flt3*$^{ITD/ITD}$ mouse model and FLT3-ITD+ primary AML blasts, we first showed that FLT3-ITD has a previously unrecognized two-fold (de)regulatory activity on the miRNA biogenesis by blocking canonical mechanisms for intron-hosted miRNAs like miR-126 and activating "non-canonical" mechanisms for long noncoding (lnc) RNA-hosted miRNAs like miR-155. The net result is a strong miRNA-mediated signal for leukemia growth.

Materials and Methods

Human and mouse samples

Normal and AML peripheral blood (PB) and BM samples were obtained, respectively, from donors and patients at the City of Hope National Medical Center (COHNMC), under one of three City of Hope Institutional Review Board approved banking protocols, #06229, #03162, #07047 or #18067 in accordance with an assurance filed with and approved by the Department of Health and Human Services, and met all requirements of the Declaration of Helsinki. Written informed consent was obtained from donors (#06229) or patients (#03162, #07047 or #18067) prior to specimen acquisition.

MNCs were isolated using Ficoll separation. CD34^{+} cells were then isolated using a positive magnetic bead selection protocol (Miltenyi Biotech, Germany). To normalize for FLT3-ITD levels in our experiments, we selected only patient samples with high FLT3-ITD allelic ratios (≥0.7). All FLT3-ITD-negative samples are also FLT3-TKD negative.

The *Mll*$^{PTD/wt}$/*Flt3*^{ITDITD} AML mouse model was used in this study [18]. Lin^{-}Sca-1^{-}c-Kit^{-} (L^{-}S^{-}K^{-}), Lin^{-}Sca-1+c-Kit- (L^{-}S+K-), Lin^{-}Sca-1^{-}c-Kit^{+} (L^{-}S^{-}K^{+}) and LSK (Lin-Sca-1+c-Kit+) cells were sorted and used for *in vitro* studies. Mouse care and experimental procedures were performed in accordance with federal guidelines and protocols and were approved by the Institutional Animal Care and Use Committee at the City of Hope.

Immunoprecipitation and Immunoblotting analyses

Cells were washed and harvested in ice-cold PBS and subsequently lysed in RIPA buffer containing 10 mM protease inhibitor cocktail (Thermo Scientific, Lafayette, CO). For immunoprecipitation, 500 μg – 1 mg of cell lysate were incubated with indicated antibody for overnight at 4°C. 50 μl of Protein A/G agarose beads (Cell Signaling, Danvers, MA) were added and the mixture was inverted for 3 hours at 4°C. For immunoblotting, immunoprecipitated complex or 50 μg of each cell lysate was separated on NuPAGE 4–12% gradient gels (Invitrogen, Carlsbad, CA) and immunocomplexes were visualized with enhanced chemiluminescence reagent (Thermo Scientific, Lafayette, CO).

miRNA labeling and analysis

The cells were cultured and incubated with a miRNA SmartFlare RNA probe (EMD Millipore) for 16 h. To ensure that the cell types, including MV-4–11 and primary AML blasts, could effectively endocytose the SmartFlare probes, we examined the uptake of probes in these cells using a SmartFlare uptake control, a scrambled control and a housekeeping 18S control (according to the manufacturer's guidelines). Cells were then washed in 1× phosphate buffered saline (PBS) and fixed in 4% paraformaldehyde for 3 min. Nuclei were counterstained with 4′,6-diamidino-2-phenylindole (DAPI), and the images were analyzed using a confocal microscope (Zeiss LSM880). A more detailed protocol is provided in Supplementary Materials and Methods.

Statistical analysis

Where indicated, to compare the means of two groups, results were generally compared by using unpaired, two-tailed Student's *t* test, with values from at least two independent experiments with triplicate determination. Data are presented as mean ± standard error (*SE*), as indicated. $p < 0.05$ was considered statistically significant; ns indicates not significant.

An extensive description of the methods can be found in the Supplementary Materials and Methods.

Target sequences for siRNAs are shown in Supplementary Table S1. TaqMan gene expression assays used for quantitative polymerase chain reaction (q-PCR) analysis are shown in Supplementary Table S2. Primer sequences used for RNA immunoprecipitation (RIP), RT-PCR and q-PCR analysis are shown in Supplementary Table S3. Antibodies used for RIP, immunoprecipitation (IP) and immunoblotting (IB) analysis are shown in Supplementary Table S4. Locked nucleic acid (LNA) probes used for fluorescent in situ hybridization (FISH) and Northern blot are shown in Supplementary Table S5. Proteins used for in vitro kinase assay are shown in Supplementary Table S6. Characteristics of patient samples are shown in Supplementary Table S7.

Results

FLT3-ITD-induced miR-126 down-regulation

We previously reported that miR-126 is downregulated in CML, via the aberrant TK activity of BCR/ABL. Low levels of miR-126 induce leukemic cells out of quiescence and contribute to leukemia growth [16]. Thus, we postulated here a similar activity for FLT3-ITD in AML. To prove this hypothesis, firstly we compared miR-126 expression levels in FLT3-ITD+ (n=55) *vs* FLT3-ITD negative (−) (n=126) AML patients from The Cancer Genome Atlas (TCGA) miRNA sequencing (seq) database [17] (Fig. 1a, left) and in primary bone marrow (BM) CD34+ blasts from AML patients' samples banked at our institution (Fig. 1a, right). We observed that levels of miR-126 were significantly lower in FLT3-ITD+ compared to FLT3-ITD- patients. Patients with FLT3-tyrosine kinase domain (TKD) point mutations were excluded from this analysis. The AML cell line MV-4–11, which carries a high FLT3-ITD allelic ratio, also expressed lower levels of miR-126 when compared with FLT3-ITD- AML cell lines (Supplementary Fig. S1A, left), normal CD34+ cells, and

FLT3-ITD- AML blasts (Supplementary Fig. S1A, right). Expression levels of miR-126 were also significantly lower in distinct immunophenotypic leukemic cell subpopulations sorted from the BM of a murine model of Flt3-ITD+ AML (*Mll*$^{PTD/wt}$/*Flt3*$^{ITD/ITD}$) [18] compared to their normal counterparts from wild-type (wt) controls (Fig. 1b).

Consistent with previous reports showing that miR-126 controls cell quiescence [12,15,16], miR-126 knock down (KD) led to an increase in cell cycling of *Mll*$^{PTD/wt}$/*Flt3*$^{ITD/ITD}$ AML LSK cells (Supplementary Fig. S1B). In contrast, miR-126 overexpression (OE) increased the percentage of quiescent AML LSK cells (Supplementary Fig. S1C). Transduction of a FLT3-ITD lentiviral vector in normal murine LSK cells decreased miR-126 levels compared with a control vector (Fig. 1c). Conversely, pharmacologic inhibition of FLT3-ITD with the TKI AC220 (quizartinib) [19] increased miR-126 expression in human primary FLT3-ITD+ blasts and cell line (MV-4–11) cells but not in human FLT3-ITD- AML blasts, normal HSCs or FLT3-ITD- cell line (HL-60) (Fig. 1d and Supplementary Fig. S1D). These results were corroborated by live miR-126 staining with SmartFlare probes (Fig. 1e and Supplementary Fig. S1E).

While we observed lower levels of mature miR-126 (Fig. 1f, left) in FLT3-ITD+ compared with FLT3-ITD- cells, we noted a reverse pattern of expression for pri-miR-126 and pre-miR-126, which were found to be higher in FLT3-ITD+ compared with FLT3-ITD- cells (Fig. 1f, middle and right). Furthermore, treatment with AC220 increased levels of mature miR-126 (Fig. 1d) and decreased levels of pri- and pre-miR-126 in FLT3-ITD+ AML blasts (Fig. 1g) and MV-4–11 cells (Supplementary Fig. S1F) but not in FLT3-ITD- cells. These findings supported our hypothesis that FLT3-ITD downregulates miR-126 by interfering with pre-miRNA processing and completion of the cytoplasmic steps of miRNA biogenesis.

FLT3-ITD disrupts canonical mechanisms of miRNA biogenesis via SPRED1 phosphorylation

One “gatekeeper” of canonical miRNA biogenesis is the XPO5/RAN-GTP complex [20]. Within this complex, XPO5 is a RAN-GTP-dependent double-stranded (ds) RNA-binding protein that mediates nuclear export of pre-miRNAs from the nucleus to the cytoplasm for the completion of miRNA maturation [21]. RAN is a small GTPase that plays a key role in determining the directionality of transport of pre-miRNAs from nucleus to cytoplasm according to a GDP-to-GTP gradient [22]. Importantly, RAS small GTPases interact and are inhibited by the SPRED1, a protein encoded by the sprouty related Drosophila enabled/vasodilator-stimulated phosphoprotein homology 1 (EVH1) domain containing 1 (*SPRED1*) gene, which is also a putative substrate for TKs and a proven target of miR-126 [23,24,25,26]. Quintanar-Audelo M et al (2011) showed that tyrosine phosphorylation is important for the interplay of SPRED1 with small GTPases [25]. Thus, we hypothesize that FLT3-ITD could inhibit the XPO5/RAN-GTP complex via SPRED1.

To this end, we first demonstrated the interaction between SPRED1 and FLT3. We showed that SPRED1 and FLT3 interacted in cell-free *in vitro* binding (Supplementary Fig. S2A) and kinase phosphorylation assays (Fig. 2a) that used recombinant proteins. Next, we showed that SPRED1 also interacted and co-localized with RAN in FLT3-ITD+ AML blasts using confocal immunostaining imaging (Supplementary Fig. S2B), Duolink protein

interaction (Fig. 2b, left) and immunoprecipitation assays (Fig. 2b, middle). We also confirmed that SPRED1 bound to RAN but not to XPO5 in a cell-free *in vitro* binding assay (Fig. 2b, right and Supplementary Fig. S2C).

Consistent with previous findings showing that SPRED1 inhibits small GTPAses via the GTPase-activating proteins (GAPs) [27], we demonstrated that SPRED1 interacted with RANGAP1, a GAP for RAN (Supplementary Fig. S2D, left), which enhanced SPRED1-RAN binding (Supplementary Fig. S2D, right). Depletion of RANGAP1 (but not that of XPO5) attenuated SPRED1 and RAN binding (Supplementary Fig. S2E). The presence of EVH1 domain, but not that of other functional SPRED1 domains [i.e., c-KIT binding domain (KBD) or cysteine-rich domain (CRD)], was required for the interaction of SPRED1 with RAN/RANGAP1 (Fig. 2c and Supplementary Fig. S2F). Mutation of SPRED1 at the Y377 and Y420 residues resulted in decreased SPRED1 and RANGAP1/RAN binding in both of MV-4–11 and HL-60 cells (Supplementary Fig. S2G), suggesting that SPRED1 phosphorylation is required for these protein-protein interactions.

Consistent with these results, higher levels of total SPRED1, p-SPRED1 and SPRED1-RAN binding were observed in FLT3-ITD+ *vs* FLT3-ITD- AML blasts (Fig. 2d). SPRED1 KD increased RAN and XPO5 interaction (Fig. 2e, top panels) and levels of mature miR-126 and reduced those of pre-miR-126 (Fig. 2e, bottom panels and Supplementary Fig. S2H) in FLT3-ITD+ AML blasts, thus supporting the inhibitory activity of p-SPRED1 on the RAN/XPO5 complex.

Taken together, these results demonstrate that FLT3-ITD downregulates miR-126 by interfering with the canonical steps of miRNA biogenesis mediated by the XPO5/RAN-GTP complex via p-SPRED1. We also show first that p-SPRED1 has GAP-activity for RAN.

miR-155 escapes the FLT3-ITD-dependent blockage of miRNA biogenesis

We and others have reported that miR-155, a multifunctional miRNA involved in regulation of hematopoiesis, immunity, inflammation and cancer growth, is overexpressed in FLT3-ITD+ AML and contributes to leukemic blast hyperproliferation and survival in molecular subsets of the disease [8,9,10,11]. However, since we showed that FLT3-ITD inhibits the XPO5/RAN-GTP complex, which reportedly processes the majority of pre-miRNAs [21,28], we reasoned that activation of mechanisms circumventing the XPO5/RAN-GTP blockage must be activated in order to promote high levels of miR-155 in FLT3-ITD+ blasts.

To explain how FLT3-ITD differentially impacted the expression levels of distinct miRNAs (i.e., decrease for miR-126 and increase for miR-155), we first noticed that, while miR-126 is hosted in an intronic region of the epidermal growth factor like domain 7 *(EGFL7)* coding gene, miR-155 is hosted at the locus of the lnc-RNA BIC-155. BIC-155 is reportedly transcribed under the control of nuclear factor kappa B (NFκB) [29,30,31,32,33], one of the downstream effectors of FLT3-ITD [9]. The lnc-RNA BIC-155 is transcribed as a 12-kb unspliced precursor RNA and subsequently spliced into a polyadenylated ≈1.7-kb pre-miRNA transcript before being processed into mature miR-155, presumably via canonical DROSHA- and Dicer-dependent mechanisms of miRNA biogenesis [29,30,31,32,33]. We noted that levels of spliced BIC-155 were lower in FLT3-ITD+ than in FLT3-ITD- AML

blasts, and that they increased upon treatment with the TKI AC220 or siAKT (Fig. 3a), thereby suggesting that FLT3-ITD may affect the BIC-155 splicing process.

Non-canonical mechanism of miR-155 biogenesis requires DDX3X/hnRNP U and NXF1

Members of the DEAD-box helicase family (DDX proteins) have been reported to control the expression of several specific miRNAs implicated in neuronal differentiation (i.e., miR-26a/b, miR-9, and miR-181a/b) [34]. DDX3X is a member of the RNA helicase protein family and is involved in the regulation of RNA splicing, and possibly in miRNA biogenesis [35,36]. Dolde et al. (2018) recently showed that phosphorylation decreases DDX3X ATPase activity, which is reportedly coupled with the helicase activity of this protein [37,38]. To this end, we noted that DDX3X harbors an AKT consensus phosphorylation motif around the S590 residue (Fig. 3b, left) and therefore we postulated that it may serve as a substrate of p-AKT, a known downstream effector of FLT3-ITD [39] (Fig. 3b, right). Consistent with this observation, we showed that the ATPase activity of DDX3X was attenuated in FLT3-ITD+ cells (Fig. 3c right, second and third bars). Conversely, treatment with the TKI AC220 or AKT KD increased both the expression (Fig. 3c, left) and the ATPase activity of DDX3X (Fig. 3c, right, third to fifth bars). Upon suppression of endogenous DDX3X in FLT3-ITD- AML blasts, forced expression of the activated GFP-AKT (AKT-myr) mutant decreased the ATPase activity of co-expressed DDX3X-wt to levels comparable to those observed with the hypoactive mutant DDX3X-DQAD (Fig. 3d).

Dardenne et al. (2014) showed that DDX5 and DDX17 cooperate with heterogeneous ribonucleoprotein particle (hnRNP) proteins in RNA splicing regulation [40,41]. A role of hnRNP U has been reported in the splicing of pre-mRNAs [42,43]. Thus, we postulated that DDX3X could interact with hnRNP U in the splicing of BIC-155. To this end, we showed that DDX3X co-localized (Fig. 4a, left) and physically interacted (Fig. 4a, middle) with hnRNP U, and in turn with unspliced BIC-155 RNA (Supplementary Fig. S3A). We conducted these experiments in FLT3-ITD- AML blasts to eliminate the interference of the FLT3 mutant on the splicing complex. We showed that the interaction between the DDX3X and hnRNP U proteins did not depend on the binding of the substrate BIC-155, as it also occurred in lineage-negative (Lin-) BM cells from miR-155 KD mice and in a cell-free assay using recombinant proteins in the absence of BIC-155 (Supplementary Fig. S3B and Fig. 4a, right). DDX3X KD reduced the interaction of DDX3X with hnRNP U (Supplementary Fig. S3C) and led to increased levels of unspliced BIC-155 RNA (Supplementary Fig. S3D and S3E) and mature miR-155 (Fig. 4b, left), and decreased levels of pri- and pre-miR-155 (Fig. 4b, right). Forced expression of DDX3X wt, the nonfunctional mutant DDX3X DQAD, or the constitutively AKT-phosphorylated mutant DDX3X S590D increased the binding of BIC-155 to hnRNP U (Fig. 4c, left), but only DDX3X wt increased BIC-155 splicing (Fig. 4c, right). KD of hnRNP U reversed the effects of DDX3X wt OE (Fig. 4d). Thus, we concluded that both proteins were required for an efficient substrate splicing. Interestingly, DDX3X activity (Fig. 3c), binding of BIC-155 RNA to hnRNP U (Fig. 4e, middle, first panel; Supplementary Fig. S3F) and BIC-155 RNA splicing (Fig. 3a) were all decreased in FLT3-ITD+ compared with FLT3-ITD- AML blasts. Accordingly, AC220 treatment or AKT KD increased the DDX3X and hnRNP U interaction (Fig. 4e, left) and BIC-155 RNA

splicing (Fig. 4e) in FLT3-ITD+ AML blasts, supporting the inhibitory role of FLT3-ITD on BIC-155 splicing.

In addition to inhibition of BIC-155 splicing, we also observed higher levels of cytoplasmic unspliced BIC-155 in FLT3-ITD+ AML compared with FLT3-ITD- AML blasts (Fig. 5a, left and 5b, second lane), as shown using fractionated RT-PCR and *in situ* hybridization. Conversely, both AC220 treatment and AKT KD, a downstream effector of FLT3-ITD, increased levels of spliced BIC-155 and reduced those of unspliced BIC-155 in FLT3-ITD+ AML blasts (Fig. 5a, right). Thus, we hypothesized that FLT3-ITD promoted an increased nucleus-to-cytoplasm transport of unspliced BIC-155. To this end, we observed an increased binding of unspliced BIC-155 to the nuclear RNA export factor 1 (NXF1) protein in FLT3-ITD+ AML blasts (Fig. 5c, left). Lipopolysaccharide (LPS) is a known activator of NFκB that reportedly promotes BIC-155 transcription [29,30,31]. To this end, we showed that LPS treatment increased enrichment of NFκB onto the BIC-155 promoter (Supplementary Fig. S4A, left) and enhanced BIC-155 mRNA expression (Supplementary Fig. S4A, right). As NXF1 binds RNA transcripts and shuttles them from the nucleus to the cytoplasm [44], NXF1 KD led to an increased nuclear retention of unspliced BIC-155 mRNA (Fig. 5d and 5e) and decreased levels of mature miR-155 (Fig. 5f) in LPS-treated FLT3-ITD+ MV-4–11 cells. Treatment with AC220 also decreased both BIC-155 mRNA-NXF1 binding and levels of mature miR-155 (Fig. 5c, right) in FLT3-ITD+ AML blasts.

As expected, NXF1 or SPRED1 KD in FLT3-ITD+ AML blasts induced cell cycle arrest and reduced cell proliferation, consistent with downregulation of mature miR-155 and upregulation of miR-126 (Supplementary Fig. S5). In contrast, DDX3X KD in FLT3-ITD+ blasts increased cell cycle and cell proliferation consistent with upregulation of miR-155 and downregulation of miR-126 (Supplementary Fig. S5).

Thus, altogether, these results support an active role of FLT3-ITD in increasing unspliced BIC-155 that is transported to the cytoplasm by NXF1. Interestingly, similar findings were also observed for other lncRNA-hosted miRNAs previously implicated in hematopoiesis and/or leukemogenesis (miR-125b, miR-196b, miR-146a) (Supplementary Fig. S4B and S4C, left), but not for intron-hosted miRNA (miR-126, miR-146b) (Fig. 5f and Supplementary Fig. S4C, right), suggesting that the described mechanisms may not be restricted respectively to BIC-155 and miR-126, but could be broadened to other miRNAs [45,46,47,48].

BIC-155 lncRNA is processed by cytoplasmic DROSHA into mature miR-155 in FLT3-ITD+ AML blasts

Having shown that unspliced BIC-155 is transported from the nucleus to the cytoplasm via NXF1, we then asked if it could also be processed into mature miR-155 in the cytoplasm of FLT3-ITD+ AML cells. DROSHA is a primarily nuclear ribonuclease that cleaves pri-miRNAs in order to produce pre-miRNAs, which are then transported to the cytoplasm where they serve as Dicer substrates in the final steps of miRNA biogenesis [49]. However, recent studies reported that some DROSHA isoforms (DROSHA 1 and 4) may localize preferentially to the cytoplasm [50,51]. Thus, we first measured the fractionated nuclear and cytoplasmic expression of DROSHA in FLT3-ITD+ and FLT3-ITD- AML blasts (Fig. 6a

and 6b, left) and normal CD34+ cells (Fig. 6a and 6b, right). Higher levels of cytoplasmic DROSHA were present in FLT3-ITD+ compared with FLT3-ITD- AML blasts and normal CD34+ cells (Fig. 6a and 6b). Furthermore, in FLT3-ITD+ MV-4–11 cells, we observed that the isoforms DROSHA 1 and DROSHA 4 preferentially localized to the cytoplasm compared with the isoforms DROSHA 2 and DROSHA 3, which instead preferentially localized to the nucleus (Supplementary Fig. S6A) [50]. Using RNA-binding protein immunoprecipitation (RIP) assays, we then proved that unspliced BIC-155 preferentially co-localized and bound with cytoplasmic DROSHA whereas pri-miR-126 colocalized with nuclear DROSHA in FLT3-ITD+ MV-4–11 cells (Supplementary Fig. S6B and S6C). Of note, we observed similar patterns of localization with cytoplasmic DROSHA for other known miRNA-hosting lncRNAs (NED-125b, MIR3142HG, and HOXA10-AS), and localization with nuclear DROSHA for other intron-hosted pri-miRs (e.g., pri-miR-146b) (Supplementary Fig. S6D).

Upon endogenous DROSHA KD and forced expression of distinct ectopic DROSHA isoforms, we observed higher levels of lncRNA-hosted miRNAs (i.e., miR-155, miR-125b, miR-146a and miR-196b; Fig. 6c-6e) in FLT3-ITD+ MV-4–11 cells transduced with DROSHA 1 and 4 (cytoplasmic isoforms) compared to those transduced with DROSHA 2 and 3 (nuclear isoforms). In contrast, forced expression of DROSHA 2 and DROSHA 3 more than that of DROSHA 1 and 4 increased levels of mature forms of intron-hosted miRNAs (i.e., miR-126 and miR-146b) (Fig. 6c, 6d and 6f). RIP assays demonstrated that BIC-155 and other lncRNAs (i.e., NED-125b, and HOXA10-AS) were preferentially bound to DROSHA 1 and 4 rather than to DROSHA 2 and 3 (Supplementary Fig. S6E) in FLT3-ITD+ MV-4–11 cells. Upon endogenous DROSHA KD, ectopically expressed DROSHA 4, but not that of DROSHA 2, increased levels of mature miR-155 from a transduced lncRNA BIC-155 vector (Supplementary Fig. S6F).

We validated these results in vivo by comparing BM Lin- MNCs from FLT3-wt with those from FLT3-ITD ($Mll^{PTD/wt}/Flt3^{ITD/ITD}$) mice (Fig. 7a). We observed that in BM Lin- MNCs from the $Mll^{PTD/wt}/Flt3^{ITD/ITD}$ mouse, DDX3X expression (Fig. 7b) and BIC-155 splicing were reduced (Fig. 7c) whereas the binding between unspliced BIC-155 and NXF1 (Supplementary Fig. S7A) and the expression of cytoplasmic BIC-155 were increased (Supplementary Fig. S7B) compared with FLT3-wt counterpart. Finally, cytoplasmic DROSHA (Fig. 7d and Supplementary Fig. S7C) and mature miR-155 (Fig. 7e) were also increased in BM Lin- MNCs from the $Mll^{PTD/wt}/Flt3^{ITD/ITD}$ mouse compared to those of FLT3-wt control.

Discussion

The miRNAs miR-126 and miR-155 have been previously reported to control, respectively, cell quiescence and proliferation both in normal hematopoiesis and leukemia [11,13,15,16,52]. Using an AML mouse model and primary blasts, we report here on a previously unrecognized function of FLT3-ITD that takes control of mechanisms of miRNA biogenesis and aberrantly upregulate miRNAs like miR-155 that promote leukemia growth and suppress those like miR-126 that contribute to cell quiescence.

We showed that FLT3-ITD decreases the biogenesis of the tumor suppressor miR-126 by interfering with pre-miR-126 processing via SPRED1 phosphorylation. Phosphorylated SPRED1 binds RAN via RANGAP1 and inhibits the XPO5-RAN complex that controls the canonical transport mechanisms of pre-miR-126 from the nucleus to the cytoplasm. This in turn results in a decreased production of mature miR-126. Since SPRED1 is a miR-126 target [26], a negative feedback regulatory loop is activated, with progressively lower levels of miR-126 that lead to progressively higher levels of SPRED1 in leukemia cells that exit quiescence, enter the cell cycle and expand. Phosphorylation is necessary for the interaction of SPRED1 with RAN in the XPO5-RAN complex and occur directly via FLT3-ITD. Of note, analysis of potential phosphorylation sites using Data from NetPhos 3.1 server-Technical University of Denmark [53 and unpublished data] support the notion that SPRED1 is a substrate for multiple kinases including PKC, CKI and CKII, c-KIT, EGFR and AKT.

Since the XPO5/RAN-GTP “gatekeeper” complex reportedly controls not only the biogenesis of miR-126 but also other miRNAs (e.g. miR-146b; Supplementary Fig. S4C) [1], it was surprising to us that miR-155 remained upregulated in FLT3-ITD+ AML blasts. Thus, we postulated that FLT3-ITD activates alternative mechanisms of miRNA biogenesis that circumvent the XPO5/RAN-GTP blockage. To this end, we noticed that, while miR-126 is hosted at the intronic region of the coding gene *EGFL7*, miR-155 is instead hosted at the lncRNA BIC-155 locus, and therefore, once transcribed, the biogenesis of these two miRNAs may follow different processing paths. Thus, while the intron-hosted miR-126 is transcribed as a pri-miRNA and then processed by nuclear DROSHA into pre-miR-126, lnc-RNA BIC-155 undergoes DDX3X splicing in normal cells. However, in AML blasts, FLT3-ITD inhibits DDX3X-dependent lncRNA BIC-155 splicing and therefore increase the levels of unspliced BIC-155. Unspliced BIC-155 binds to NXF1 and is transported to the cytoplasm, where it serves as a substrate for cytoplasmic DROSHA for completion of BIC-155 maturation into miR-155 (Fig. 7f), thereby by-passing the XPO5/RAN-GTP blockage. Of note, the existence of cytoplasmic DROSHA was recently reported in cancer cell lines [50,51], and here first shown in primary leukemic blasts. Thus, our study supports the notion of a dual activity of FLT3-ITD on miRNA biogenesis that leads to aberrantly decrease in miR-126 to overcome cell quiescence and aberrantly increase in miR-155 to promote leukemia growth

Of note, the mechanisms of FLT3-ITD-dependent disruption of miRNA biogenesis also affect intron-hosted miRNAs other than miR-126, and lncRNA-hosted miRNAs other than miR-155 (see Fig. 5 and Supplementary Fig. S4). However, generalization of this observation to the whole miRNome of cancer cells requires additional studies. In fact, the high cellular specificity of miRNA expression, high degree of overlap between gene- and lncRNA-hosted miRNAs (e.g. some miRNAs are hosted in lncRNAs that overlap with introns of coding genes), and the difference in levels of aberrantly activated kinases, may differentially impact the degree by which miRNA biogenesis is dysregulated. Nevertheless, as miRNA-targeting therapeutics are being explored in the clinic [54], the aberrant activity of FLT3-ITD on miRNA biogenesis could provide opportunities for adding novel miRNA-targeting therapeutic approaches to the current therapeutic armamentarium available for the treatment of these AML patients.

Supplementary Material

Refer to Web version on PubMed Central for supplementary material.

Acknowledgments

We are grateful to Dr. Sven Diederichs and Dr. Gu Shuo for DROSHA constructs, Dr. Yixian Zheng for RAN constructs, and Dr. Paul Taylor for DDX3X constructs and Dr. Marjorie Robbins for editing the manuscript. This work was supported by CA205247, CA201184, Jerome Foundation (G.M.) and Hoag Foundation (G.M.). This work was partially supported by Natural Science Foundation of Zhejiang Province, China (LQ18H080001); National Natural Science Foundation of China (No. 81800146). Research reported in this publication included work performed in the City of Hope Hematopoietic Tissue Biorepository (Pathology Research Services Core) supported by the National Cancer Institute of the National Institutes of Health under grant number P30CA033572. The content is solely the responsibility of the authors and does not necessarily represent the official views of the National Institutes of Health.

References

1. Ha M, Kim VN. Regulation of microRNA biogenesis. Nat Rev Mol Cell Biol. 2014;15:509–24. [PubMed: 25027649]
2. Garzon R, Garofalo M, Martelli MP, Briesewitz R, Wang L, Fernandez-Cymering C, et al. Distinctive microRNA signature of acute myeloid leukemia bearing cytoplasmic mutated nucleophosmin. Proc Natl Acad Sci U S A. 2008;105:3945–50. [PubMed: 18308931]
3. Liao Q, Wang B, Li X, Jiang G. miRNAs in acute myeloid leukemia. Oncotarget. 2017;8:3666–82. [PubMed: 27705921]
4. Marcucci G, Radmacher MD, Maharry K, Mrozek K, Ruppert AS, Paschka P, et al. MicroRNA expression in cytogenetically normal acute myeloid leukemia. N Engl J Med. 2008;358:1919–28. [PubMed: 18450603]
5. Wallace JA, O'Connell RM. MicroRNAs and acute myeloid leukemia: therapeutic implications and emerging concepts. Blood. 2017;130:1290–301. [PubMed: 28751524]
6. Daver N, Schlenk RF, Russell NH, Levis MJ. Targeting FLT3 mutations in AML: review of current knowledge and evidence. Leukemia. 2019;33:299–312. [PubMed: 30651634]
7. Stone RM, Mandrekar SJ, Sanford BL, Laumann K, Geyer S, Bloomfield CD, et al. Midostaurin plus Chemotherapy for Acute Myeloid Leukemia with a FLT3 Mutation. N Engl J Med. 2017;377:454–64. [PubMed: 28644114]
8. Marcucci G, Maharry KS, Metzeler KH, Volinia S, Wu YZ, Mrozek K, et al. Clinical role of microRNAs in cytogenetically normal acute myeloid leukemia: miR-155 upregulation independently identifies high-risk patients. J Clin Oncol. 2013;31:2086–93. [PubMed: 23650424]
9. Gerloff D, Grundler R, Wurm AA, Brauer-Hartmann D, Katzerke C, Hartmann JU, et al. NF-kappaB/STAT5/miR-155 network targets PU.1 in FLT3-ITD-driven acute myeloid leukemia. Leukemia. 2015;29: 535–47. [PubMed: 25092144]
10. Wallace JA, Kagele DA, Eiring AM, Kim CN, Hu R, Runtsch MC, et al. miR-155 promotes FLT3-ITD-induced myeloproliferative disease through inhibition of the interferon response. Blood. 2017;129:3074–86. [PubMed: 28432220]
11. Narayan N, Bracken CP, Ekert PG. MicroRNA-155 expression and function in AML: An evolving paradigm. Exp Hematol. 2018;62:1–6. [PubMed: 29601851]
12. de Leeuw DC, Denkers F, Olthof MC, Rutten AP, Pouwels W, Schuurhuis GJ, et al. Attenuation of microRNA-126 expression that drives CD34+38- stem/progenitor cells in acute myeloid leukemia leads to tumor eradication. Cancer Res. 2014;74:2094–105. [PubMed: 24477595]
13. Dorrance AM, Neviani P, Ferenchak GJ, Huang X, Nicolet D, Maharry KS, et al. Targeting leukemia stem cells in vivo with antagomiR-126 nanoparticles in acute myeloid leukemia. Leukemia. 2015;29:2143–53. [PubMed: 26055302]
14. Lechman ER, Gentner B, van Galen P, Giustacchini A, Saini M, Boccalatte FE, et al. Attenuation of miR-126 activity expands HSC in vivo without exhaustion. Cell Stem Cell. 2012;11:799–811. [PubMed: 23142521]

15. Lechman ER, Gentner B, Ng SW, Schoof EM, van Galen P, Kennedy JA, et al. miR-126 Regulates Distinct Self-Renewal Outcomes in Normal and Malignant Hematopoietic Stem Cells. Cancer Cell. 2016;29:214–28. [PubMed: 26832662]
16. Zhang B, Nguyen LXT, Li L, Zhao D, Kumar B, Wu H, et al. Bone marrow niche trafficking of miR-126 controls the self-renewal of leukemia stem cells in chronic myelogenous leukemia. Nat Med. 2018;24:450–62. [PubMed: 29505034]
17. Cancer Genome Atlas Research N, Ley TJ, Miller C, Ding L, Raphael BJ, Mungall AJ, et al. Genomic and epigenomic landscapes of adult de novo acute myeloid leukemia. N Engl J Med. 2013;368:2059–74. [PubMed: 23634996]
18. Zorko NA, Bernot KM, Whitman SP, Siebenaler RF, Ahmed EH, Marcucci GG, et al. Mll partial tandem duplication and Flt3 internal tandem duplication in a double knock-in mouse recapitulates features of counterpart human acute myeloid leukemias. Blood. 2012;120:1130–6. [PubMed: 22674806]
19. Zarrinkar PP, Gunawardane RN, Cramer MD, Gardner MF, Brigham D, Belli B, et al. AC220 is a uniquely potent and selective inhibitor of FLT3 for the treatment of acute myeloid leukemia (AML). Blood. 2009;114:2984–92. [PubMed: 19654408]
20. Roberts TC. The MicroRNA Biology of the Mammalian Nucleus. Mol Ther Nucleic Acids. 2014;3:e188. [PubMed: 25137140]
21. Bohnsack MT, Czaplinski K, Gorlich D. Exportin 5 is a RanGTP-dependent dsRNA-binding protein that mediates nuclear export of pre-miRNAs. RNA. 2004;10:185–91. [PubMed: 14730017]
22. Okamura M, Inose H, Masuda S. RNA Export through the NPC in Eukaryotes. Genes (Basel). 2015;6:124–49. [PubMed: 25802992]
23. Wakioka T, Sasaki A, Kato R, Shouda T, Matsumoto A, Miyoshi K, et al. Spred is a Sprouty-related suppressor of Ras signalling. Nature. 2001;412:647–51. [PubMed: 11493923]
24. Brems H, Pasmant E, Van Minkelen R, Wimmer K, Upadhyaya M, Legius E, et al. Review and update of SPRED1 mutations causing Legius syndrome. Hum Mutat. 2012; 33:1538–46. [PubMed: 22753041]
25. Quintanar-Audelo M, Yusoff P, Sinniah S, Chandramouli S, Guy GR. Sprouty-related Ena/vasodilator-stimulated phosphoprotein homology 1-domain-containing protein (SPRED1), a tyrosine-protein phosphatase non-receptor type 11 (SHP2) substrate in the Ras/extracellular signal-regulated kinase (ERK) pathway. J Biol Chem. 2011;286:23102–12.
26. Wang S, Aurora AB, Johnson BA, Qi X, McAnally J, Hill JA, et al. The endothelial-specific microRNA miR-126 governs vascular integrity and angiogenesis. Dev Cell. 2008;15:261–71. [PubMed: 18694565]
27. Fuhrer S, Ahammer L, Ausserbichler A, Scheffzek K, Dunzendorfer-Matt T, Tollinger M. NMR resonance assignments of the EVH1 domain of neurofibromin's recruitment factor Spred1. Biomol NMR Assign. 2017;11:305–8. [PubMed: 28831766]
28. Lund E, Guttinger S, Calado A, Dahlberg JE, Kutay U. Nuclear export of microRNA precursors. Science. 2004;303:95–8. [PubMed: 14631048]
29. Elton TS, Selemon H, Elton SM, Parinandi NL. Regulation of the MIR155 host gene in physiological and pathological processes. Gene. 2013;532:1–12. [PubMed: 23246696]
30. Eis PS, Tam W, Sun L, Chadburn A, Li Z, Gomez MF, et al. Accumulation of miR-155 and BIC RNA in human B cell lymphomas. Proc Natl Acad Sci U S A. 2005;102:3627–32. [PubMed: 15738415]
31. Gatto G, Rossi A, Rossi D, Kroening S, Bonatti S, Mallardo M. Epstein-Barr virus latent membrane protein 1 trans-activates miR-155 transcription through the NF-kappaB pathway. Nucleic Acids Res. 2008;36:6608–19. [PubMed: 18940871]
32. Rai D, Karanti S, Jung I, Dahia PL, Aguiar RC. Coordinated expression of microRNA-155 and predicted target genes in diffuse large B-cell lymphoma. Cancer Genet Cytogenet. 2008;181: 8–15. [PubMed: 18262046]
33. Tam W Identification and characterization of human BIC, a gene on chromosome 21 that encodes a noncoding RNA. Gene. 2001;274:157–67. [PubMed: 11675008]

34. Lambert MP, Terrone S, Giraud G, Benoit-Pilven C, Cluet D, Combaret V, et al. The RNA helicase DDX17 controls the transcriptional activity of REST and the expression of proneural microRNAs in neuronal differentiation. Nucleic Acids Res. 2018;46:7686–700. [PubMed: 29931089]
35. Zhao L, Mao Y, Zhao Y, He Y. DDX3X promotes the biogenesis of a subset of miRNAs and the potential roles they played in cancer development. Sci Rep. 2016;6:32739.
36. Lossner C, Meier J, Warnken U, Rogers MA, Lichter P, Pscherer A, et al. Quantitative proteomics identify novel miR-155 target proteins. PLoS One. 2011;6:e22146.
37. Dolde C, Bischof J, Gruter S, Montada A, Halekotte J, Peifer C, et al. A CK1 FRET biosensor reveals that DDX3X is an essential activator of CK1epsilon. J Cell Sci. 2018;131(1).
38. Valentin-Vega YA, Wang YD, Parker M, Patmore DM, Kanagaraj A, Moore J, et al. Cancer-associated DDX3X mutations drive stress granule assembly and impair global translation. Sci Rep. 2016;6:25996.
39. Brandts CH, Sargin B, Rode M, Biermann C, Lindtner B, Schwable J, et al. Constitutive activation of Akt by Flt3 internal tandem duplications is necessary for increased survival, proliferation, and myeloid transformation. Cancer Res. 2005;65:9643–50. [PubMed: 16266983]
40. Dardenne E, Polay Espinoza M, Fattet L, Germann S, Lambert MP, Neil H, et al. RNA helicases DDX5 and DDX17 dynamically orchestrate transcription, miRNA, and splicing programs in cell differentiation. Cell Rep. 2014;7:1900–13. [PubMed: 24910439]
41. Fu XD, Ares M, Jr. Context-dependent control of alternative splicing by RNA-binding proteins. Nat Rev Genet. 2014;15:689–701. [PubMed: 25112293]
42. Vu NT, Park MA, Shultz JC, Goehe RW, Hoeferlin LA, Shultz MD, et al. hnRNP U enhances caspase-9 splicing and is modulated by AKT-dependent phosphorylation of hnRNP L. J Biol Chem. 2013;288:8575–84. [PubMed: 23396972]
43. Ye J, Beetz N, O'Keeffe S, Tapia JC, Macpherson L, Chen WV, et al. hnRNP U protein is required for normal pre-mRNA splicing and postnatal heart development and function. Proc Natl Acad Sci U S A. 2015;112:E3020–29.
44. Gruter P, Tabernero C, von Kobbe C, Schmitt C, Saavedra C, Bachi A, et al. TAP, the human homolog of Mex67p, mediates CTE-dependent RNA export from the nucleus. Mol Cell. 1998;1:649–59. [PubMed: 9660949]
45. Rodriguez A, Griffiths-Jones S, Ashurst JL, Bradley A. Identification of mammalian microRNA host genes and transcription units. Genome Res. 2004;14:1902–10. [PubMed: 15364901]
46. Bevilacqua V, Gioia U, Di Carlo V, Tortorelli AF, Colombo T, Bozzoni I, et al. Identification of linc-NeD125, a novel long non coding RNA that hosts miR-125b-1 and negatively controls proliferation of human neuroblastoma cells. RNA Biol. 2015;12:1323–37. [PubMed: 26480000]
47. Shaham L, Binder V, Gefen N, Borkhardt A, Izraeli S. MiR-125 in normal and malignant hematopoiesis. Leukemia. 2012;26:2011–8. [PubMed: 22456625]
48. Paterson MR, Kriegel AJ. MiR-146a/b: a family with shared seeds and different roots. Physiol Genomics. 2017;49:243–52. [PubMed: 28213571]
49. Kuehbacher A, Urbich C, Zeiher AM, Dimmeler S. Role of Dicer and Drosha for endothelial microRNA expression and angiogenesis. Circ Res. 2007;101:59–68. [PubMed: 17540974]
50. Link S, Grund SE, Diederichs S. Alternative splicing affects the subcellular localization of Drosha. Nucleic Acids Res. 2016;44:5330–43. [PubMed: 27185895]
51. Dai L, Chen K, Youngren B, Kulina J, Yang A, Guo Z, et al. Cytoplasmic Drosha activity generated by alternative splicing. Nucleic Acids Res. 2016;44:10454–66.
52. Li Z, Chen P, Su R, Li Y, Hu C, Wang Y, et al. Overexpression and knockout of miR-126 both promote leukemogenesis. Blood. 2015;126:2005–15. [PubMed: 26361793]
53. Blom N, Sicheritz-Ponten T, Gupta R, Gammeltoft S, Brunak S. Prediction of post-translational glycosylation and phosphorylation of proteins from the amino acid sequence. Proteomics. 2004;4:1633–49. [PubMed: 15174133]
54. Hanna J, Hossain GS, Kocerha J. The Potential for microRNA Therapeutics and Clinical Research. Front Genet. 2019;10:478. [PubMed: 31156715]
55. Kortylewski M, Swiderski P, Herrmann A, Wang L, Kowolik C, Kujawski M, et al. In vivo delivery of siRNA to immune cells by conjugation to a TLR9 agonist enhances antitumor immune responses. Nat Biotechnol. 2009;27:925–32. [PubMed: 19749770]

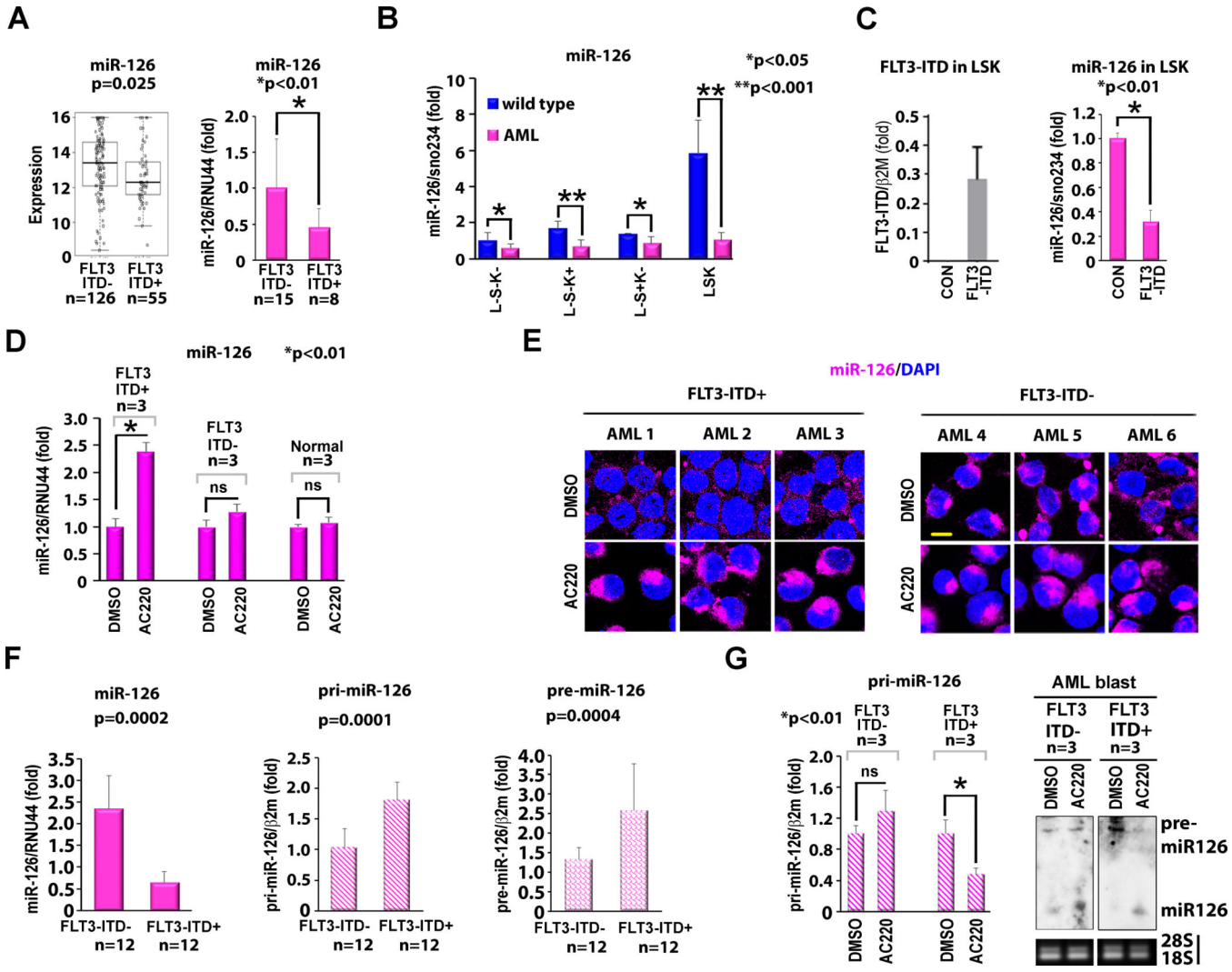

Fig. 1: FLT3-ITD down-regulates miR-126 expression.

a miR-126 expression in FLT3-ITD+ vs FLT3-ITD- AML patients from a public database (left) and in BM primary CD34+ blasts (right). For BM primary CD34+ blasts, total RNA was extracted and levels of miR-126 were measured by q-PCR. **b** Comparison of miR-126 levels in BM MNC immunophenotypic subpopulations from wild type (wt) *vs* *Mll*$^{PTD/wt}$/*Flt3*$^{ITD/ITD}$ AML mice. BM MNCs were isolated from each group of mice and subpopulations were isolated using flow cytometry (as described in Methods). MiR-126 expression was measured by q-PCR; (each group, n=3). **c** LSK cells from wt mice (n=3) transduced with control (CON) or FLT3-ITD lentivirus vectors. FLT3-ITD (left) and miR-126 (right) expression levels were measured by q-PCR at 48 hours. **d, e** miR-126 expression in CD34+ blasts from healthy donor or FLT3-ITD- *vs* FLT3-ITD+ AML patients treated *ex-vivo* with DMSO (CON) or the tyrosine kinase inhibitor AC220 (20 nM) measured by q-PCR (**d**) or staining with SmartFlare miR-126 probes (**e**). The cells were treated with DMSO or AC220 for 24 hours. **f** Mature miR-126 (left), pri-miR-126 (middle), and pre-miR-126 (right) expression in FLT3-ITD- (n=12) and FLT3-ITD+ (n=12) AML blasts. Levels of pri-, pre- and mature miR-126 were measured by q-PCR. **g** FLT3-ITD-

and FLT3-ITD+ AML blasts (each group, n=3) were treated with DMSO or 20 nM AC220 for 24 hours. Left, pri-miR-126 by q-PCR. Right, Northern blot to detect pre-miR-126 and mature miR-126. Unless otherwise noted, results from triplicate experiments are shown, error bars represent SD. Significance was calculated using unpaired t test, “p” values are shown. Scale bar, 10 μm.

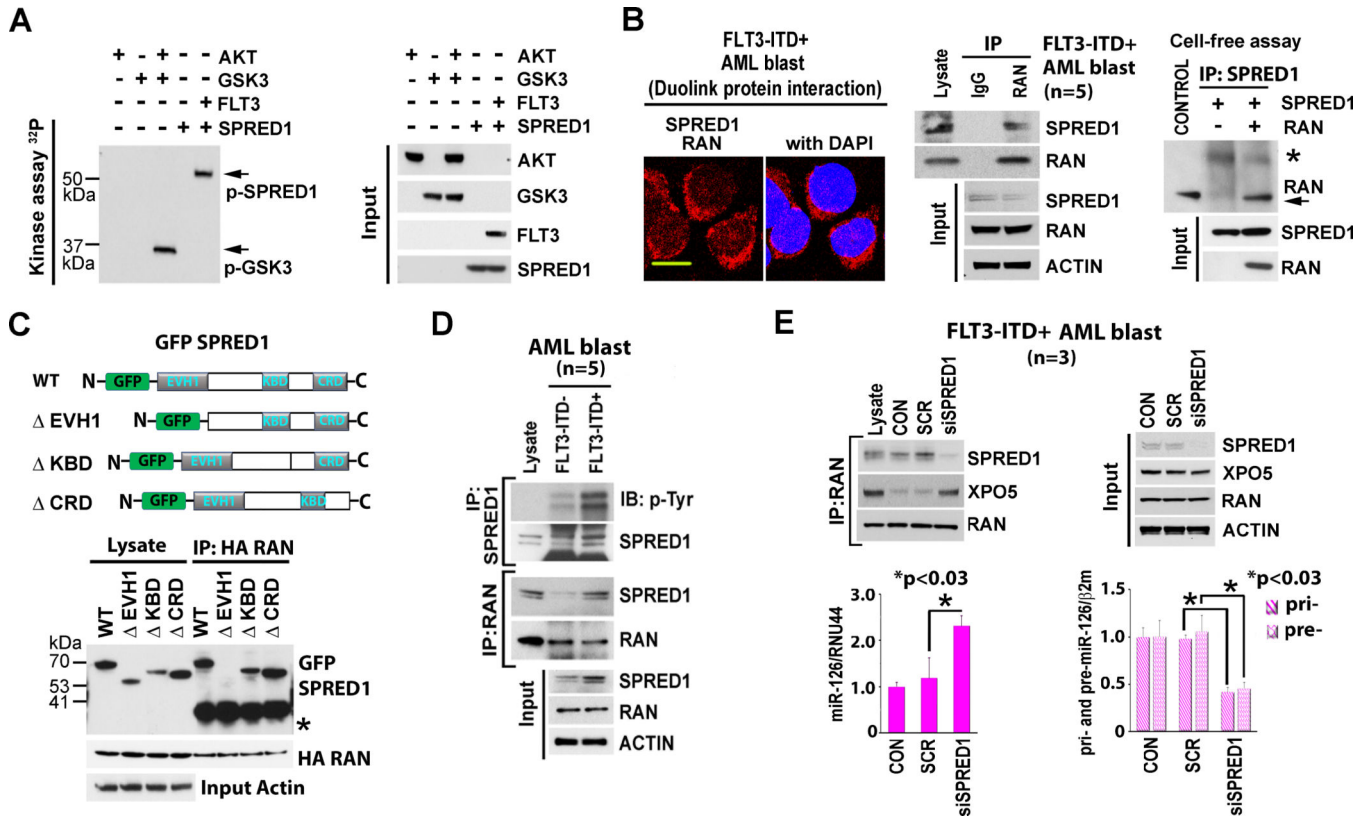

Fig. 2: Inhibition of XPO5/RAN by SPRED1.

a SPRED1 phosphorylation by FLT3. Cell-free *in vitro* kinase phosphorylation assay performed using AKT, GSK3, FLT3, and SPRED1 recombinant proteins. AKT phosphorylated GSK3 was used as a positive control for the phosphorylation assay. Left, phosphorylation of SPRED1 and GSK3. Right, input controls of recombinant proteins using in kinase assay. **b** Interaction between SPRED1 and RAN in FLT3-ITD+ AML blasts demonstrated by Duolink protein interaction assay (left) and co-immunoprecipitation assay (middle). For immunoprecipitation assay, the lysate was immunoprecipitated with anti-IgG control or anti-RAN antibodies and immunoblotted with anti-SPRED1 and anti-RAN antibodies. Input controls are shown. Right, direct interaction of SPRED1 and RAN demonstrated by cell-free binding assay with recombinant proteins. SPRED1 and RAN recombinant proteins were incubated in the binding buffer overnight and the complex was immunoprecipitated with anti-SPRED1 antibody and immunoblotted with anti-RAN antibody. *, nonspecific band. **c** Mapping binding domain of SPRED1 with RAN. Top, schematic presentation of the SPRED1 constructs used to map the binding domain of SPRED1 on RAN as shown on bottom. Bottom, immunoprecipitation of GFP-SPRED1 proteins overexpressed together with HA-RAN in MV-4–11 cells using anti-HA and anti-GFP antibodies. Input controls of protein expression are shown. **d** SPRED1 phosphorylation and SPRED1 and RAN physical interaction in FLT3-ITD- *vs* FLT3-ITD+ AML blasts. Five samples of each group were pooled for the assay. The lysate was immunoprecipitated with anti-SPRED1 or anti-RAN antibodies and immunoblotted with indicated antibodies. **e** Effects of SPRED1 knock down (KD) by siRNAs (40 nM) on miR-126. FLT3-ITD+ AML blasts (n=3) were transfected with siSCR or siSPRED1 for 24 hours. Top, interaction

of SPRED1, RAN and XPO5 determined by immunoprecipitation. Three samples of each group were pooled for the assay. Input controls are shown on the right. Bottom, miR-126 and pri- and pre-miR-126 expression as assessed by q-PCR. Unless otherwise noted, results from triplicate experiments are shown, error bars represent SD. Significance was calculated using unpaired t test, “p” values are shown. Scale bar, 10 μm.

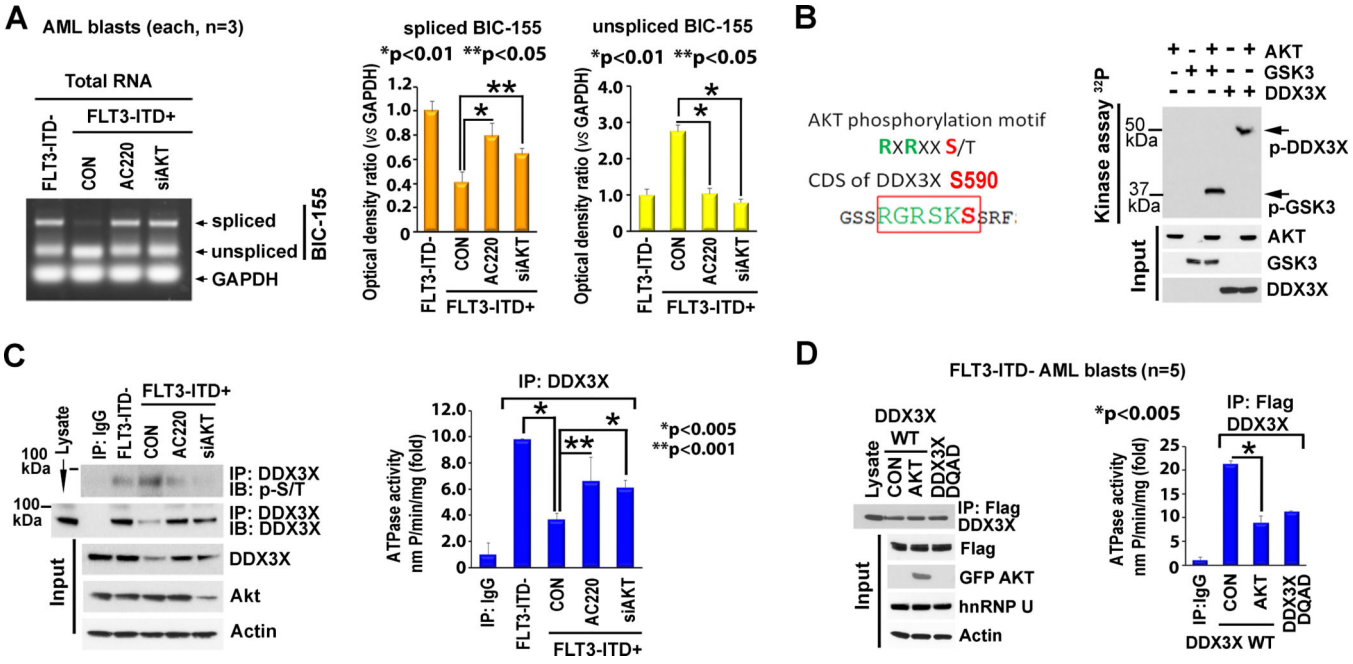

Fig. 3: Regulation of DDX3X activities in FLT3-ITD cells.

a BIC-155 unspliced and spliced levels in FLT3-ITD- and FLT3-ITD+ AML blasts. The FLT3-ITD- or FLT3-ITD+ blasts were treated with vehicle (CON), AC220 or siAKT (each, n=3) for 24 hours and analyzed for unspliced and spliced BIC-155 expression by RT-PCR (see Methods for assay and primer sequences). Semiquantitative expression levels are shown on right. **b** AKT phosphorylates DDX3X. Left, AKT phosphorylation motif on CDS of DDX3X protein. The AKT phosphorylation motif (RXRXX-S/T) is shown at Serine 590. Right, *in vitro* phosphorylation assay using recombinant proteins of AKT, GSK3 and DDX3X. AKT phosphorylated GSK3 was used as a positive control for phosphorylation assay. Top, phosphorylation of DDX3X and GSK3. Bottom, input controls of recombinant proteins using in kinase assay. **c** DDX3X ATPase activity in FLT3-ITD- and FLT3-ITD+ AML blasts (each, n=3). Left, whole protein lysate from FLT3-ITD- or FLT3-ITD+ AML blasts were immunoprecipitated (IP) with anti-DDX3X antibody and immunoblotted with anti-phospho-Serine/Threonine antibody. Right, Fold ATPase activity is shown. **d** ATPase activity of AKT-phosphorylated DDX3X. FLT3-ITD- AML blasts (n=5) were transfected with indicated constructs for 24 hours. Left, efficacy of Flag DDX3X pull down is shown. Right, fold ATPase activity is shown. Unless otherwise noted, results from triplicate experiments are shown, error bars represent SD. Significance was calculated using unpaired t test, “p” values are shown.

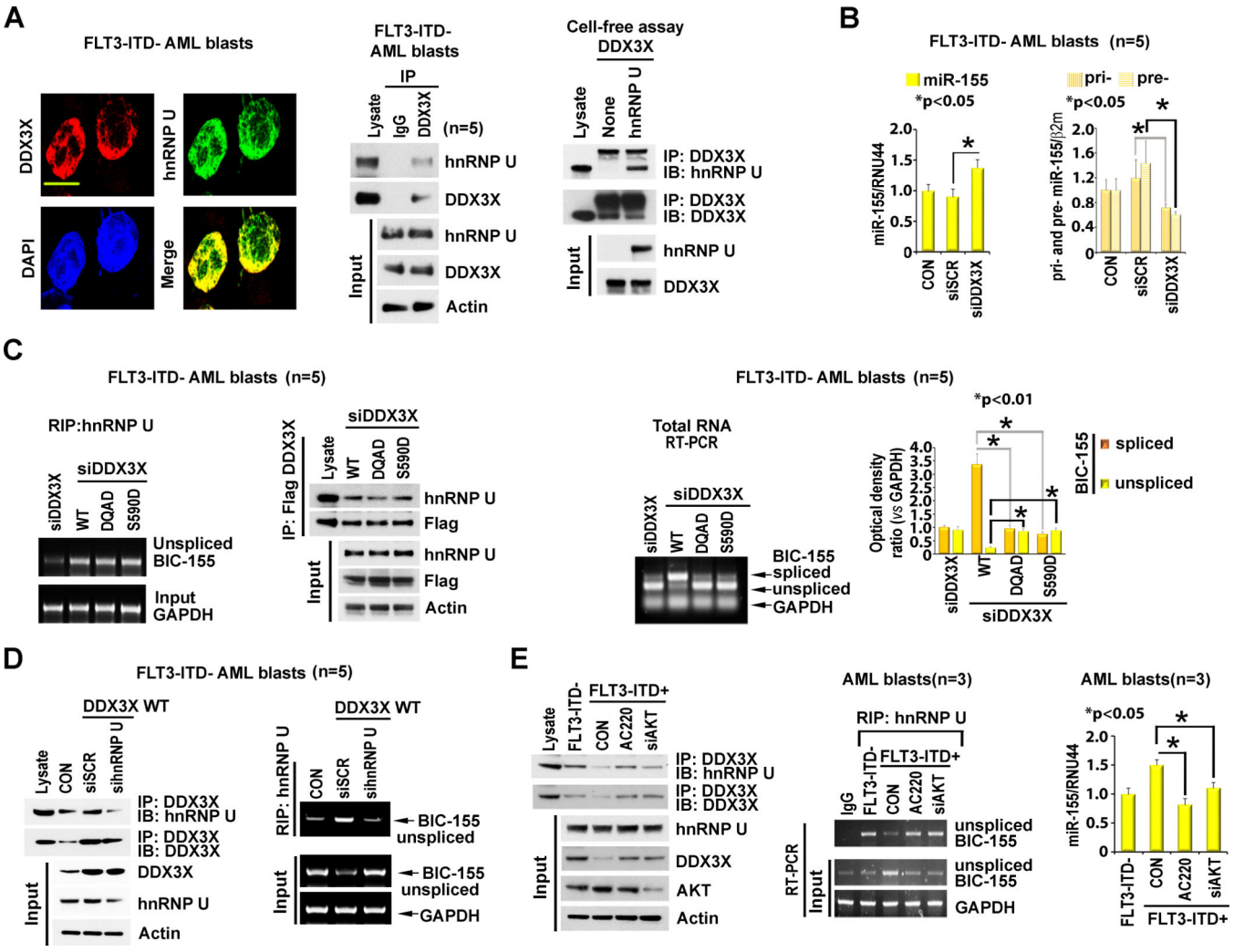

Fig. 4: Regulation of BIC-155 splicing by DDX3X and hnRNP U.

a Interaction between DDX3X and hnRNP U. Left, co-localization between DDX3X and hnRNP U in FLT3-ITD- AML blast. The cells were stained with anti-DDX3X (red) and anti-hnRNP U (green) antibodies and images were taken under confocal microscope. Pearson correlation (p) value = 0.69 ± 0.08. Middle, protein lysate from FLT3-ITD- AML blasts (n=5) was used for immunoprecipitation and immunoblotting using anti-DDX3X and anti-hnRNP U antibodies. Right, cell-free binding assay using recombinant DDX3X and hnRNP U protein. DDX3X and hnRNP U recombinant proteins were incubated in the binding buffer for overnight and the complex was immunoprecipitated with anti-DDX3X antibody and immunoblotted with anti-DDX3X and anti-hnRNP U antibodies. **b** Effects of DDX3X KD on pri-, pre- and miR-155 levels. FLT3-ITD- AML blasts (n=5) were transfected with siSCR or siDDX3X (20 nM) for 24 hours Levels of miR-155 (left), pri- and pre-miR-155 (right) were measured by q-PCR. **c** Rescued effects of DDX3X WT, DQAD or S590D mutant on siDDX3X-regulated BIC-155 splicing. The FLT3-ITD- AML blasts (n=5) were transfected with siDDX3X (20 nM) and then continuously transfected with DDX3X WT, DQAD or S590D mutant. Left, interaction between unspliced BIC-155 and hnRNP U (by RIP assay, see Methods) and IP and IB controls. Right, expression of spliced

and unspliced forms of BIC-155 by RT-PCR. Optical density ratio is shown. **d** Effects of hnRNP U KD on DDX3X regulated BIC-155 splicing. FLT3-ITD- AML blasts (n=5) were transfected with DDX3X WT in the presence of siSCR or sihnRNP U (20 nM) for 24 hours. The interaction of DDX3X and hnRNP U are on the left and levels of unspliced BIC-155 binding with hnRNP U and total unspliced BIC-155 are on the right. **e** Different levels of DDX3X binding with hnRNP U and miR-155 expression between FLT3-ITD- and FLT3-ITD+ AML blasts (each, n=3). Left, interaction between DDX3X and hnRNP U determined by IP. Middle, the levels of unspliced BIC-155 bound to hnRNP U determined by RIP assay. Right, miR-155 levels determined by q-PCR. Unless otherwise noted, results from triplicate experiments are shown, error bars represent SD. Significance was calculated using unpaired t test, “p” values are shown. Scale bar, 10 μm.

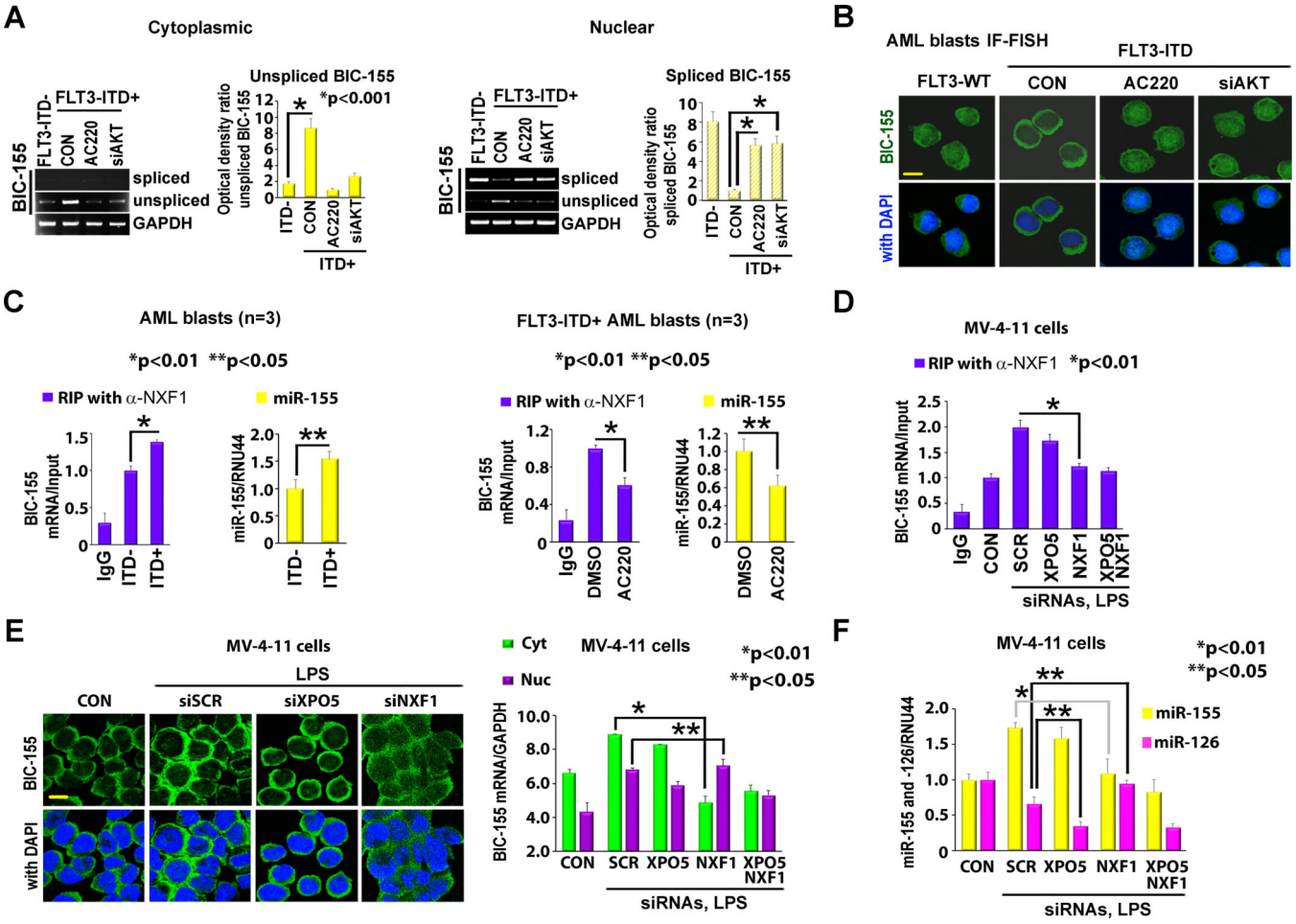

Fig. 5: Lnc-RNA hosted miR-155 transportation by NXF1.

a, b Fractionated cytoplasm and nuclear distribution of unspliced BIC-155 in FLT3-ITD+ AML blasts. **a** The cells were fractionated into cytoplasmic and nuclear fraction. Expression of unspliced and spliced BIC-155 in indicated cells were assessed by RT-PCR. Densitometry quantification of RT-PCR results of unspliced BIC-155 and spliced BIC-155 are shown. **b** *In situ* hybridization was performed on the indicated cells with specific probes targeting BIC-155. Representative images are shown. **c** BIC-155/NXF1 binding in FLT3-ITD- and FLT3-ITD+ AML blasts. Left, the FLT3-ITD- or FLT3-ITD+ blasts (each, n=3) were analyzed for levels of BIC-155 binding to NXF1 using RNA-binding protein immunoprecipitation (RIP) assay (see Methods) and miR-155 using q-PCR. Right, the FLT3-ITD+ blasts (n=3) were treated with AC220 or vehicle for 24 hours and interaction of BIC-155/NXF1 and miR-155 levels were analyzed. **d-f** Effects of NXF1 KD on cellular distribution of BIC-155 and expression of miRNAs. MV-4–11 cells were treated with LPS for 24 hours in the presence of siSCR, siXPO5, or siNXF1. **d** Interaction between BIC-155 and NXF1 by RIP assay. **e** Left, cell images with *in situ* hybridization of BIC-155. Right, quantitative analysis of cellular distribution of BIC-155. **f** Levels of miR-126 and miR-155 were measured by q-PCR. Significance was calculated using unpaired t test, “p” values are shown. Scale bar, 10 μm.

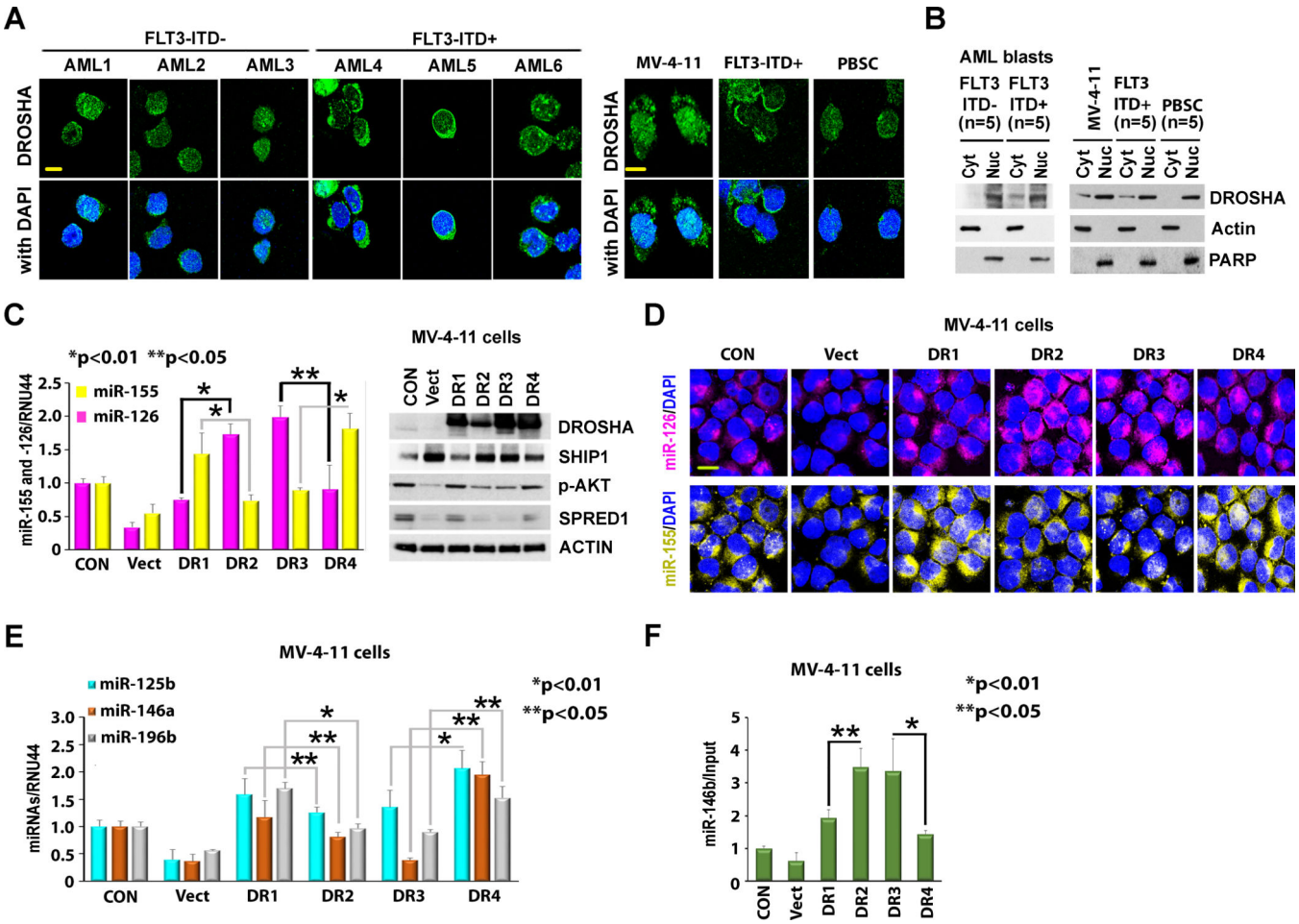

Fig. 6: Lnc-RNA hosted miR-155 processing by cytoplasmic DROSHA.

a, b Cellular distribution of DROSHA in FLT3-ITD-, FLT3-ITD+ AML blasts and normal peripheral blood mononuclear cells (PBMC). **a** Representative image of DROSHA staining in three individual FLT3-ITD- and FLT3-ITD+ AML blasts (left) and in MV-4–11 cells, FLT3-ITD+ AML blast, and PBMC cells (right). The images were taken under confocal microscope. **b** Immunoblot of cellular fractionation with indicated antibodies. The indicated cells were fractionated to cytoplasmic and nuclear fractions and immnublotting was performed with indicated antibodies. **c, d** Effects of DROSHA isoforms on miR-126 and miR-155 expression. MV-4–11 cells were transfected with siDROSHA to knock down (KD) expression of endogenous DROSHA and then transfected with each DROSHA isoform to assess the role of the individual isoforms. **c** Expression levels of miR-126 and miR-155 by q-PCR is shown on (left). Right, control immunoblotting with indicated antibodies. **d** Representative images of cells staining with indicated miRNA SmartFlare probes (see Methods). **e, f** Effects of DROSHA isoforms on intronic and lnc-RNA hosted miRNAs expression. MV-4–11 cells were transfected as described in (**c**, **d**). Expression levels of lnc-RNA-hosted miRNAs by q-PCR is shown on (**e**) and that of intronic miR-146b on (**f**). Unless otherwise noted, results from triplicate experiments are shown, error bars represent SD. Significance was calculated using unpaired t test, “p” values are shown. Scale bar, 10 μm.

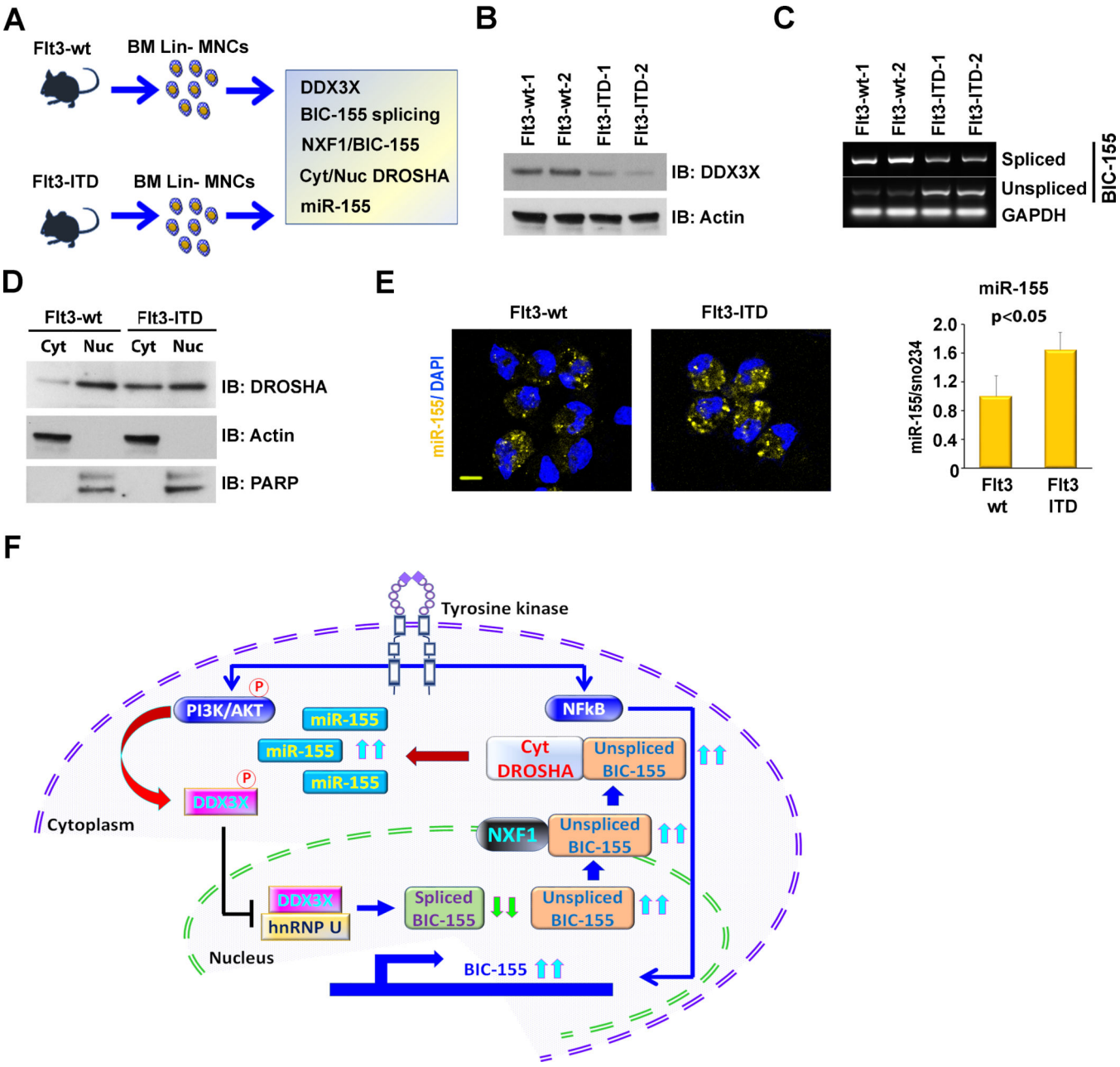

Fig. 7: Regulation of miR-155 processing by DDX3X/NXF1/cytoplasmic DROSHA in BM Lin- cells from Flt3-ITD mice.

a *In vivo* experimental design. The lineage-negative (Lin-) stem-progenitor cell population from BM were isolated from Flt3 wild type (wt) or Flt3-ITD (*Mll*$^{PTD/wt}$/*Flt3*$^{ITD/ITD}$) mice to analyze as indicated (each group, n=3). **b, c** Expression of DDX3X and BIC-155 splicing in Lin- cells from Flt3-wt and Flt3-ITD mouse. **b** Level of DDX3X was examined by immunoblotting. **c** Unspliced or spliced BIC-155 was examined by RT-PCR. **d** Cellular distribution of DROSHA in Lin- cells from Flt3-wt and Flt3-ITD mice. Immunoblot of cellular fractionation with indicated antibodies is shown. **e** Levels of miR-155 were measured by staining with SmartFlare probes (left) and q-PCR (right). **f** Schematic model

of regulation miR-155 expression in FT3-ITD+ AML cells through regulation of DDX3X/NXF1/cytoplasmic DROSHA. Unless otherwise noted, results from triplicate experiments are shown, error bars represent SD. Significance was calculated using unpaired t test, “p” values are shown. Scale bar, 10 μm.